Detection of underground installations in hostile environments

A Biosonar Application

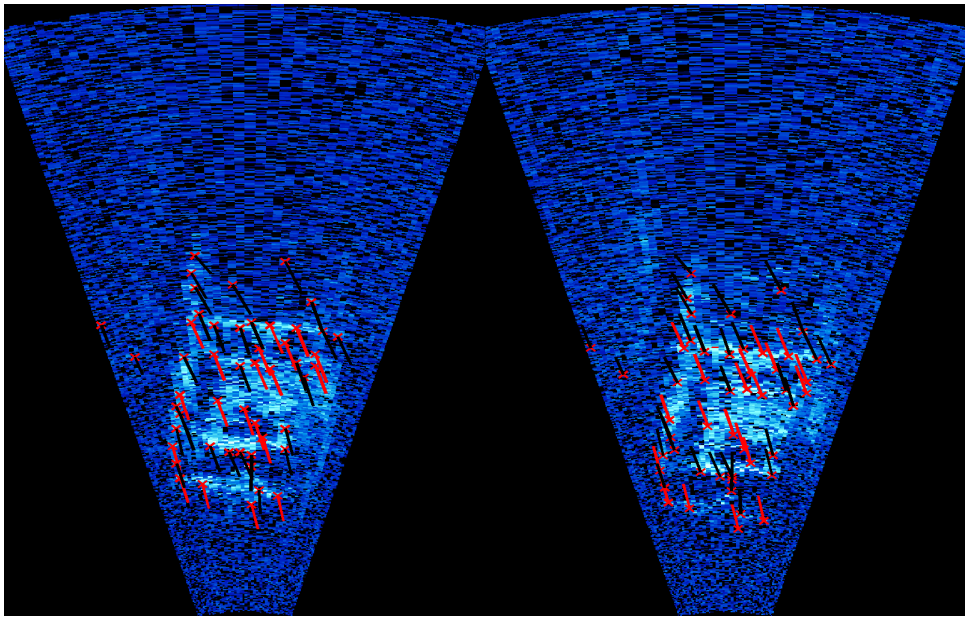

12/31/2009

Research Report

Recent hostile activities have demonstrated the importance of creating reliable and accurate information about underground activity and underground installations of any sort. While there has been great progress in acquiring intelligence on the ground, with the advancement of multi-spectral high-resolution satellite imagery, it has become evident, that once installations are buried deep under the ground, they become invisible to current intelligence gathering methods. The current research is focused on biological inspired methods for mapping sub-terrain installation using infrasound acoustic imaging ("acoustic eye").

Detection of underground installations in hostile environments

RESEARCH REPORT

1 BACKGROUND AND RESEARCH OBJECTIVES

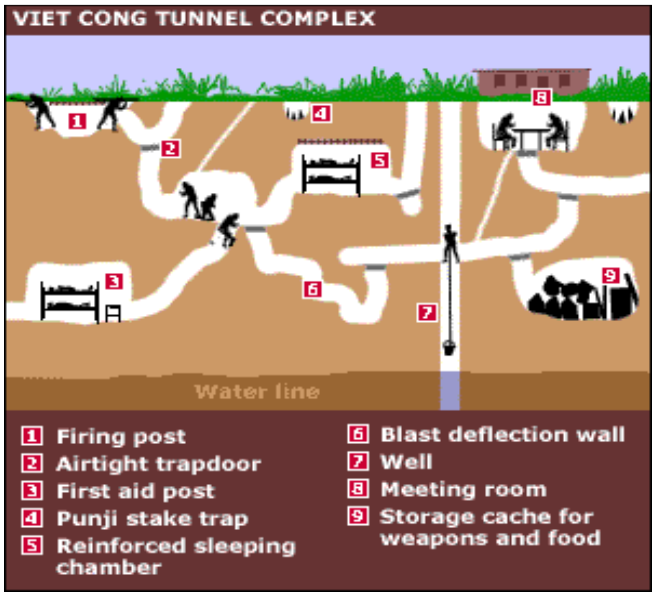

Figure 1: Underground installments

Detecting and imaging of underground installments (e.g. tunnels, bunkers) in a hostile environment poses unique challenges on deployment and remote sensing methods a detection system may employ. A system should remain undetected by the enemy and, therefore, should not use methods requiring high-energy signals. A system deployment should be fast and hassles to stay unnoticed. Sensing and imaging algorithms should be robust enough to handle heterogeneous sub-terrain properties and provide reasonable resolution of areas of interest. The system should be able to operate in fully and semi-autonomous mode to reduce amount of communications with a control center, thus, reducing a risk of being detected by an adversary.

Our approach assumes multiple sensors deployed underground with proximity to an area of interests. While underground sensor deployment has some technical difficulties, this settings provide the best solution in terms of long duration of activity without being discovered, as well as the potential ability to get as close as possible to the desired target and explore it from many aspects

This research focuses on computational and modeling methods associated with underground installment detection system. We explore methods for sub-terrain imaging using fusion of low-energy infrasound signal responses. Our work is inspired by recent discovery of remote sensing capabilities of Blind Mole Rat, which is able to detect and avoid object buried underground.

2 PREVIOUS WORK

Remote sensing and imaging in sub-terrain and marine environment have some significant civil and warfare applications .These applications have motivated numerous academic and industry research efforts. In this section, we provide brief overview on related problems and available methods.

2.1 Reflection Seismology

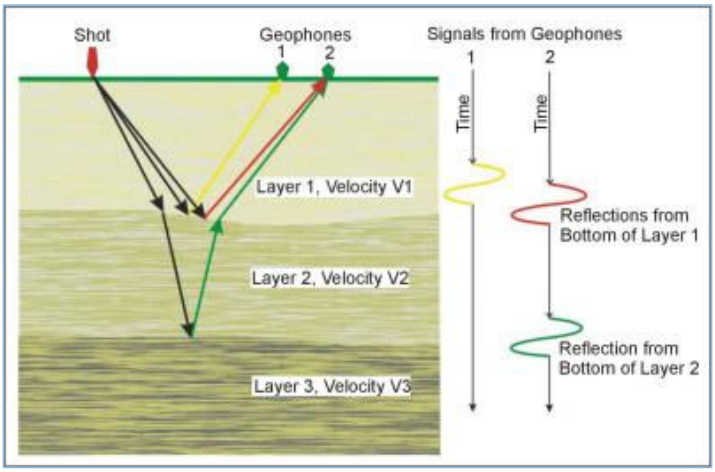

Figure 2: Reflection seismology principles

Reflection seismology (or seismic reflection) is a method of exploration geophysics that uses the principles of seismology to estimate the properties of the Earth's subsurface from reflected seismic waves. The method requires a controlled seismic source of energy, such as dynamite, a specialized air gun or vibrators, commonly known by their trademark name Vibroseis. Vibrators are large trucks that shake a vibrating pad through a known frequency band. By noting the time it takes for a reflection to arrive at a receiver, it is possible to estimate the depth of the feature that generated the reflection.

2.2 Acoustic-to-seismic coupling

When an acoustic wave strikes the ground surface, energy is coupled into motion of the fluid/solid matrix comprising the ground. The in-phase and out-of-phase motion of the fluid relative to the solid results in two compressional waves that propagate in the ground. This phenomenon is well documented and is termed acoustic-to-seismic coupling in the relevant literature**[2]**. In the ground, the pore fluid waves travel with a speed well below the speed of sound in air. The porous nature of the ground causes the entering acoustic wave to bend toward the normal and the acoustic wave propagates downwards in the ground. When an object is buried lower than a few centimeters below the ground surface, it results in distinct changes in the acoustic-to-seismic coupled motion. These changes can be sensed both on the ground surface and below the surface.

2.3 Ground Penetrating Radar

Ground-penetrating radar (GPR) is a geophysical method that uses radar pulses to image the subsurface. This non-destructive method uses electromagnetic radiation in the microwave band (UHF/VHF frequencies) of the radio spectrum, and detects the reflected signals from subsurface structures. GPR can be used in a variety of media, including rock, soil, ice, fresh water, pavements and structures. It can detect objects, changes in material, and voids and cracks. Ground-penetrating radar (GPR) is a geophysical method that uses radar pulses to image the subsurface.

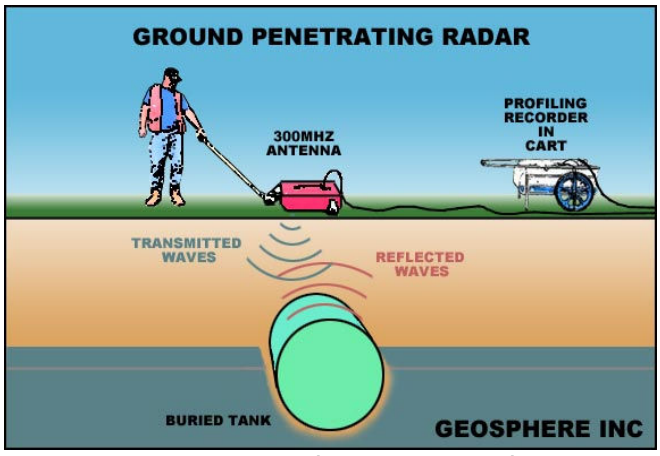

Figure 3: Ground-penetrating radar

This non-destructive method uses electromagnetic radiation in the microwave band (UHF/VHF frequencies) of the radio spectrum, and detects the reflected signals from subsurface structures. GPR uses transmitting and receiving antennas. The transmitting antenna radiates short pulses of the high-frequency (usually polarized) radio waves into the ground. When the wave hits a buried object or a boundary with different dielectric constants, the receiving antenna records variations in the reflected return signal. The principles involved are similar to reflection seismology, except that electromagnetic energy is used instead of acoustic energy, and reflections appear at boundaries with different dielectric constants instead of acoustic impedances.

The depth range of GPR is limited by the electrical conductivity of the ground, and the transmitting frequency. As conductivity increases, the penetration depth also decreases. This is because the electromagnetic energy is more quickly dissipated into heat energy, causing a loss in signal strength at depth. Higher frequencies do not penetrate as far as lower frequencies, but give better resolution. Optimal depth penetration is achieved in dry sandy soils or massive dry materials such as granite, limestone, and concrete where the depth of penetration is up to 15 m. In moist and/or clay-laden soils and soils with high electrical conductivity, penetration is sometimes only a few centimeters.

Ground-penetrating radar antennas are generally in contact with the ground for the strongest signal strength; however, GPR horn antennas can be used 0.3 to 0.6 m above the ground.

3 BIOLOGICAL MOTIVATION

3.1 Animal echolocation

Echolocation, also called Biosonar, is the biological sonar used by several mammals such as bats (although not all species), dolphins and whales (though not baleen whales).. Two bird groups also employ this system for navigating through caves, the so-called cave swiftlets in the genus Aerodramus (formerly *Collocalia*) and the unrelated Oilbird *Steatornis caripensis*. Echolocating animals emit calls out to the environment, and listen to the echoes of those calls that return from various objects in the environment.

Figure 4: Echolocating bat

They use these echoes to locate, range, and identify the objects. Echolocation is used for navigation and for foraging (or hunting) in various environments. Microbats use echolocation to navigate and forage, often in total darkness. They generally emerge from their roosts in caves or attics at dusk and forage for insects into the night. Their use of echolocation allows them to occupy a niche where there are often many insects (that come out at night since there are fewer predators then) and where there is less competition for food, and where there are fewer other species that may prey on the bats themselves. Microbats generate ultrasound via the larynx and emit the sound through the nose or, much more commonly, the open mouth. Microbat calls range in frequency from 14,000 to well over 100,000 Hz, mostly beyond the range of the human ear (typical human hearing range is considered to be from 20 Hz to 20,000 Hz). Individual bat species echolocate within specific frequency ranges that suit their environment and prey types. This has sometimes been used by researchers to identify bats flying in an area simply by recording

their calls with ultrasonic recorders known as 'bat detectors'. However, echolocation calls are not species specific and some bats overlap in the type of calls they use so recordings of echolocation calls cannot be used to identify all bats. In recent years researchers in several countries have developed 'bat call libraries' that contain recordings of local bat species that have been identified known as 'reference calls' to assist with identification.

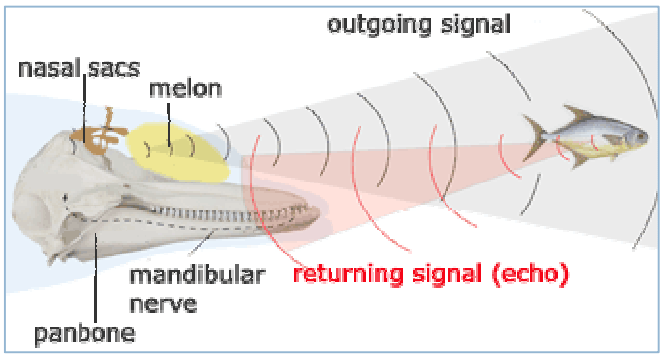

Figure 5: Biosonar of toothed whales

Toothed whales (suborder odontoceti), including dolphins, porpoises, river dolphins, orcas and sperm whales, use biosonar because they live in an underwater habitat that has favorable acoustic characteristics and where vision is extremely limited in range due to absorption or turbidity. Toothed whales emit a focused beam of high-frequency clicks in the direction that their head is pointing. A large fatty organ known as the 'melon' modulates the focused beam.

Toothed whale whistles do not appear to be used in echolocation. Different rates of click production in a click train give rise to the familiar barks, squeals and growls of the bottlenose dolphin. A click train with a repetition rate over 600 per second is called a burst pulse. In bottlenose dolphins, the auditory brain response resolves individual clicks up to 600 per second, but yields a graded response for higher repetition rates.

3.2 Blind Mole Rat

Another animal that uses sonar-like exploration of the underground is the mole rat. This rat, which lives underground and has no functioning eyes, generates ground stimulation by banging its head on the wall of its tunnels. It has been shown, that this is a sufficient stimulation for generating a full 3D view for some tens of meters neighborhood [**1**]. Since that study, it has also been shown, that tunnels of mole rates can reach a length of two miles. From behavioral studies, we learn that a mole rate finds out if some intruder got into its tunnel very quickly (as they become very aggressive).

Figure 6: Blind Mole Rat

It thus follows; that the mole rat can utilize its infrasound exploration device to a long range of over a mile. A mole rat can dig a tunnel 300ft long in one night. It runs inside the tunnel at a great speed (compared to the size of its body), thus indicating that it can "see" quite well, although its eyes are not functioning. The mole-rate bangs its head on the side of the tunnel few times per second and explores the 3D environment using the infrasound that is returned from these banging. This is reminiscent to what is done in seismic underground exploration. How are the ping returns being transformed into an image, we

do not quite know, but one can expect that a mechanism similar to the one performed by Bats, Dolphins and other biosonar animals is employed. *The bottom line is that the mole-rate proves that effective underground exploration is possible.*

4 DEPLOYMENT ALTERNATIVES

Although focus of our work is computational aspects of underground installments detection system, available sensor deployment methods have some effect on the range and characteristics of proposed processing schemes. Therefore, this section gives a brief overview of some alternatives of sub-terrain sensors deployment methods.

4.1 Sub-terrain robotics

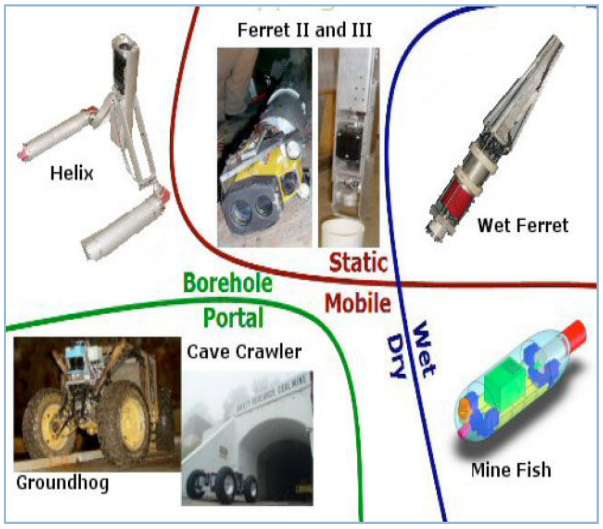

Figure 7: Sub-terrain robotic systems

Robotic systems exhibit remarkable capability for exploring and mapping subterranean voids. The spectrum of conditions encountered in subterranean spaces calls for a variety of robotic systems in response. Depending upon the target environment, a robot may need to scale rock, tread mud, sink, or swim to collect information. No single robot design could be applicable to every conceivable subterranean space; therefore, specialization is essential in subterranean robot design. The ensuing robot descriptions will be classified along three dimensions: Mobility, void accessibility, and submersion. Mobility covers actuation characteristics; void accessibility covers ingress capabilities; and submersion covers the ability to operate under water.

4.2 Remotely controlled rat navigation

A remotely guided rat, popularly called a ratbot or "robo-rat", is a rat with electrodes implanted in the medial forebrain bundle (MFB) and sensorimotor cortex of its brain. Sanjiv Talwar and John Chapin at the State University of New York Downstate Medical Center developed them in 2002. The rats wear a small electronics backpack containing a radio receiver and electrical stimulator. The rat receives remote stimulation in the sensorimotor cortex via its backpack that causes the rat to feel a sensation in its left or right whiskers, and stimulation in the MFB that is interpreted as a reward or pleasure.

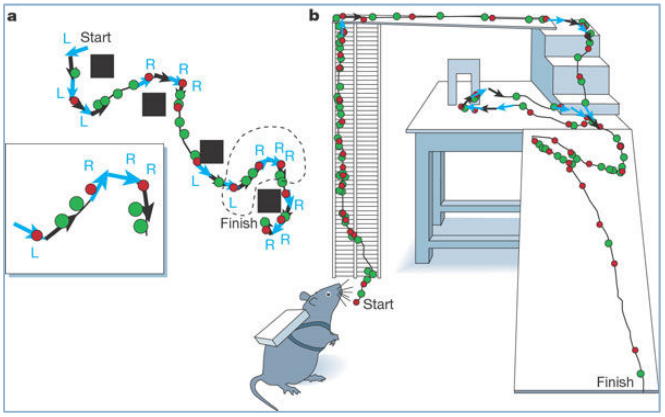

Figure 8: "a robo-rat"

After a period of training and conditioning using MFB stimulation as a reward, the rats can be remotely directed to move left, right, and forward in response to whisker stimulation signals. It is possible to roughly guide the animal along an obstacle course, jumping small gaps and scaling obstacles

4.3 Time of Arrival Estimation

In remote sensing applications such as radar or sonar, the common scenario starts by a transmitter sending out a pulse waveform $s(t)$. The pulse is reflected from a target and it is picked up by a receiver at time $\mathbf{t_0}$. The estimated two-way travel time (lag) can be used to calculate distance to the target assuming the speed of the pulse propagation in the medium is known.

The signal recorded at the receiver might be represented as

$$u(t) = c * s(t - t_o) + n(t)$$

where $n(t)$ is Additive White Gaussian Noise(AWGN) which corrupts the signal. The $c < 1$ factor is used to account for all non-free space propagation losses (e.g. attenuation of the signal in the medium). We are interested in estimating the Time of Arrival (ToA) parameter $\mathbf{t_0}$ under the assumption that noise n is large relative to **c*s(t)**.

The analysis of the performance of different time-of-arrival estimation methods is essential for Radar, Sonar and other remote sensing applications. Rather than compute the exact error of a specific estimator, it is often more convenient to lower-bound the error of any estimators for a given problem. The conventional Matched Filter Maximum Likelihood (MFML) estimator is considered efficient as it asymptotically attains the Cramer-Rao Bound (CRB) under sufficiently high SNR conditions [**10**]. However, under lower SNR levels, the Cramer-Rao Bound appears to be over-optimistic and a more tight forms of bound are required if the level of noise is high. The Barankin Bound [**9**] and associated Barankin Theory provide tools for constructing useful bounds for mean error of an estimator under low SNR. Although in its general form the Barankin bound depends on the estimated parameter and therefore can't be easily computed, it's able to account for well-known threshold phenomena in the estimation of the time-of-arrival parameter.

According to Woodward who studied the threshold effect back in 1953[**6**], it's "one of the most interesting features of radar theory". It appears that when SNR at a receiver falls below certain threshold value, the mean square error of the estimation is rapidly increasing causing dramatic drop in sensing accuracy. A receiver operating with SNR above this threshold value is said to be in a coherent state. The MFML estimator is usually used for the coherent receiver. For the SNR levels substantially below the threshold value, a receiver said to be noncoherent with the assumption that most of the pulse carrier frequency is lost due to the noise. For in-between levels of SNR, a receiver is said to be a semi-coherent receiver, balancing between coherent and noncoherent states.

The necessity and possibility of a different approach for the semi-coherent receiver had been demonstrated [**5**] for the case of multiple pulses. Often several pulses are sent to increase accuracy of remote sensing measurements. In the contrast to the conventional wisdom, it appears that averaging estimates obtained from the several measurements is not the best strategy for the semi-coherent receiver. More robust fusion statistics (e.g. mode or mean) produce better results under these circumstances.

In this paper we describe a robust single pulse ToA estimation method for semi-coherent receiver. We show how to construct a pairs of suboptimal and biased estimators. A pair of estimators is obtained using phase-shifted versions of source waveform as unmatched filters. The outcomes of an estimator pair are fused together into a single ToA estimator which outperforms MFML estimator for a range of low SNR levels. We introduce an adaptive ToA estimator by selecting phase-shift value according to anticipated SNR at a receiver.

4.4 Maximum Likelihood Matched Filter Estimator

The standard method for ToA estimation employs Matched Filter (MF) applied to the received signal. The Matched Filter maximizes peak signal to mean noise ratio [1], [7], making its output suitable for the Maximum Likelihood (ML) estimator of the ToA. The Matched Filter Maximum Likelihood (MFML) estimator of ToA is obtained by taking the position of the global maximum in the output of the Matched Filter (MF). The output of the Matched Filter can be expressed as a correlation of the signal with the pulse waveform:

$$\boldsymbol{y(t) = u(t) \circ s(t) = g(t) + h(t)}$$

Where $\boldsymbol{g(t)}$ is scaled and shifted version of the pulse's autocorrelation function and $\boldsymbol{h(t)}$ is filtered noise. A typical Gaussian-modulated sinusoidal pulse and its autocorrelation function are shown at **Figure 1**. In the absence of noise, the maximum value of $\boldsymbol{y(t)}$ is achieved at $\boldsymbol{t = t_o}$. As the level of noise increases, the filtered noise $\boldsymbol{h(t)}$ may cause a slight shift in the position of the peak of $\boldsymbol{y(t)}$ function. However, at the high noise levels, a position around one of the side lobes of $\boldsymbol{g(t)}$ may occasionally become the global maximum of $\boldsymbol{y(t)}$.

A side lobe of autocorrelation function mistakenly taken as its global maximum is a major reason behind deterioration in accuracy of MFML estimator known as threshold effect [6]. The threshold effect occurs as soon as Signal to Noise Ratio (SNR) $\boldsymbol{R}$ falls below the level that is given approximately by

$$\boldsymbol{R \sim 2\log(F * R * B)}$$

where $\boldsymbol{F}$ is the detection interval and $\boldsymbol{B}$ is the signal bandwidth.

The threshold effect manifests itself in rapid increase in the Root Mean Square Error (RMSE) of the MFML estimator as shown in the **Figure 2.** In semi-coherent state, the posteriori distribution of the possible lag locations becomes multimodal (**Figure 3**) because of the significant height of autocorrelation function's side lobes. The height of the side lobes of autocorrelation function as affected by a pulse bandwidth and, therefore the threshold effect is considerable for low-frequency narrowband pulses. Under these circumstances, the Maximal Likelihood

4.5 Unmatched Filter Maximum Likelihood Estimators

Given an arbitrary pulse waveform $\boldsymbol{s(t)}$ we construct a pair of Phase Shifted Unmatched (PSU) filters $\boldsymbol{f_{\varphi}^{+}(t)}$ and $\boldsymbol{f_{\varphi}^{-}(t)}$ by shifting phase of the pulse by $+\boldsymbol{\varphi}$ and $-\boldsymbol{\varphi}$ respectively. A Gaussian-modulated sinusoidal pulse and its PSU filter pair generated using $\boldsymbol{\varphi = \frac{\pi}{2}}$ are shown in **Figure 4.** The cross correlation of the signal $\boldsymbol{u(t)}$ and a PSU pair's filter can be expressed as:

$$\mathbf{y_{\varphi}^{\pm}(t) = u(t) \circ f_{\varphi}^{\pm}(t) = g_{\varphi}^{\pm}(t) + h_{\varphi}^{\pm}(t)}$$

The Unmatched Filter Maximum Likelihood (UFML) estimators $\boldsymbol{t_{\varphi}^{-}}$ and $\boldsymbol{t_{\varphi}^{+}}$ corresponding to a PSU pair can be defined as:

$$\boldsymbol{t_{\varphi}^{\pm} = argmax\left(y_{\varphi}^{\pm}(t)\right) = argmax(u(t) \circ f_{\varphi}^{\pm}(t))}$$

The side lobes of the cross-correlation function $\mathbf{g_{\varphi}^{\pm}(x) = s(t) \circ f_{\varphi}^{\pm}(t)}$ have unequal heights, making UFML estimators biased toward the higher side lobe as shown in **Figure 5**. The bias of the two UFML estimators has equal absolute value but opposite sign due to symmetry in the heights and position of the cross-correlation side lobes. As SNR is increased, the bias decreases since the position of the cross-correlation maximum is less affected by the noise. Note that autocorrelation and PSU filter cross-correlation produce signals of the same power, however application of unmatched filter produces lower peak signal-to-mean-noise ratio as compared to matched filter.

The Root Mean Square Error (RMSE) of a single UFML estimator is higher as compared to the RMSE of MFML as shown at **Figure 6**. However, the UFML estimators corresponding to a PSU filter pair are not perfectly correlated as can be seen at **Figure 7**. Therefore we can define a new estimator by averaging results from a pair of UFML:

$$t_{\varphi} = \frac{t_{\varphi}^{-} + t_{\varphi}^{+}}{2}$$

At low SNR levels, the resulting Average of UFML (AoUFML) estimator has lower RMSE as compared to MFML (**Figure 8**). The AoUFML estimator outperforms MFML estimator at SNR levels corresponding to semi-coherent receiver state. At higher SNR levels, the effect of side lobes is insignificant therefore the shape of the main peak of cross-correlation function have critical impact on the estimator's RMSE. Since an unmatched filter produces smaller peak signal-to-mean-noise ratio and the UFML pair is almost perfectly correlated at higher SNR levels, the MFML estimator outperform the AoUFML estimator t_{φ} at coherent receiver state. Cross-over points between AoUFML and MFML RMSE curves can be controlled by choosing appropriate phase shift parameter $\boldsymbol{\varphi}$ as described below.

4.6 Adaptive phase selection

There are two factors to take into account during the selection of the value $\boldsymbol{\varphi}$ for generating PSU filter pair. Namely, we wish to minimize correlation between the values of additive noise $\mathbf{h}_{\boldsymbol{\varphi}}^{+}(t)$ and $\mathbf{h}_{\boldsymbol{\varphi}}^{-}(t)$, while keeping peak signal-to-mean-noise level of $\mathbf{y}_{\boldsymbol{\varphi}}^{\pm}(\mathbf{t})$ close to that of Matched Filter output $y(t)$. Since the average noise level is not affected by PSU filtering, the peak SNR level depends on the height of main peak of cross-correlation function. The peak height is smaller with larger values of the phase shift $\boldsymbol{\varphi}$, meaning that $\boldsymbol{\varphi}$ should be decreased as SNR level approaches the coherent range. On the other hand, the correlation between noise phases decreases with larger phase, becoming zero when $\boldsymbol{\varphi} = \frac{\pi}{2}$ making the noise phases of $\mathbf{h}_{\boldsymbol{\varphi}}^{+}(t)$ and $\mathbf{h}_{\boldsymbol{\varphi}}^{-}(t)$ orthogonal.

In general, the optimal value of $\boldsymbol{\varphi}$ from the interval $\left[\mathbf{0}:\frac{\pi}{2}\right]$ can be selected according to estimated levels of noise present in the signal. This principle is illustrated in **Figure 8** which shows the RMSE curves for several values of $\boldsymbol{\varphi}$ and the RMSE curve corresponding do adaptively selected phase shift value $\boldsymbol{\varphi}$**.** Using curves presented in **Figure 9** and **Figure 10**, the optimal value of the phase-shift for a given pulse can be selected based on estimated level of SNR (the review of SNR estimation techniques can be found in **[8]**). The optimal value of the phase shift value used in AoUFML estimator depends on the pulse central frequency and the pulse bandwidth. A pulse with larger bandwidth have narrower envelope of the auto-correlation function. Therefore smaller values of phase shift produce larger changes in the height of a side lobe. As a result, the optimal value for AoUFML phase shift is smaller for pulses with larger bandwidth (**Figure 9**). In a similar manner, as the central frequency of the pulse is increased, the peaks of autocorrelation function become more closely spaced. Therefore larger values of phase shift can be used in UFML in order to produce significant difference in side-lobes height (**Figure 10**).

4.7 Conclusions

We showed that using Phase Shifted Unmatched (PSU) filters, a pair of Unmatched Filter Maximum Likelihood (UFML) estimators can be applied to obtain biased Time of Arrival estimators. In semi-coherent receiver state, the UFML estimators are not perfectly correlated and, therefore, can be combined together into estimator that

outperforms conventional Matched Filter Maximum Likelihood estimator. There is an optimal phase shift level that produce lowest RMSE for given SNR. Therefore a phase shift level can be selected adaptively according to estimated SNR level in order to achieve best accuracy in a semi coherent state. Since proposed estimator does not require special pulse waveform or additional pulses it can be used during a post-processing phase in remote sensing applications operating under high noise.

4.8 References

[1] A. D. Whalen, "*Detection of Signals in Noise*", Academic Press, 1995
[2] L. R. Varshney and D. Thomas, "*Sidelobe reduction for matched filter range processing*", Proceedings of IEEE Radar Conference, 2003.
[3] GP Succi, G Prado, R Gampert and TK Pedersen, "*Problems in Seismic detection and Tracking*", Proceedings of SPIE 2000.
[4]**Tali Kimchi, Moshe Reshef, Joseph Terkel,** "*Evidence for the use of reflected self-generated seismic waves for spatial orientation in a blind subterranean mammal*", Journal **of Experimental Biology** 2005
[5]L. Yu, N. Neretti, N. Intrator, "Multiple ping sonar accuracy improvement using robust motion estimation and ping fusion", JASA 2006.
[6] P. Woodward, "*Probability and Information Theory, with Applications to Radar*", McGraw-Hill, 1953
[7] Steven M. Kay, "*Fundamental of Statistical Signal Processing*", Prentice Hall, 1993
[8] D.R. Pauluzzi, N.C. Beaulieu, "*A comparison of SNR estimation techniques for the AWGN channel*", IEEE Transaction on Communications 2000.
[9] E.W. Barankin, "*Locally best unbiased estimates*" Ann Math. Statist., 20:477-501,1949
[10] Harry L. Van Treese, "*Detection, Estimation and Modulation Theory*", John Wiley & Sons, Inc. New York 1968
[11] M.I. Skolnik, "*Introduction to Radar Systems*", McGraw-Hill Book Company 1962
[12] A.Zeira and P.M. Schultheiss, "*Realizable lower bounds for time delay estimation-Part II: Threshold phenomena*" IEEE Trans. Signal Processing, May 1994

4.9 Figures

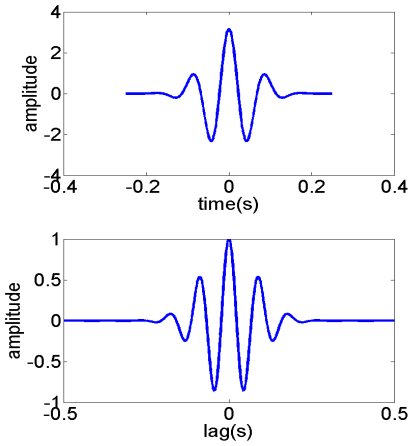

Figure 1: Gaussian modulated sinusoidal pulse(top) and its autocorrelation function

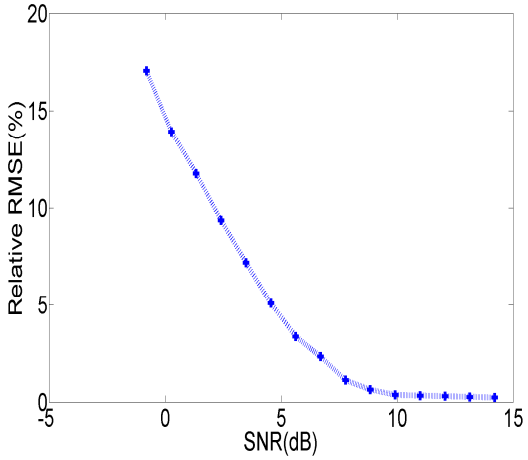

Figure 2: The MFML estimator threshold effect

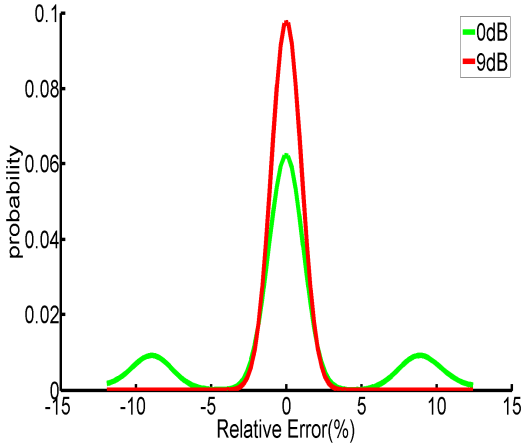

Figure 3: The probability density function for MFML estimator error

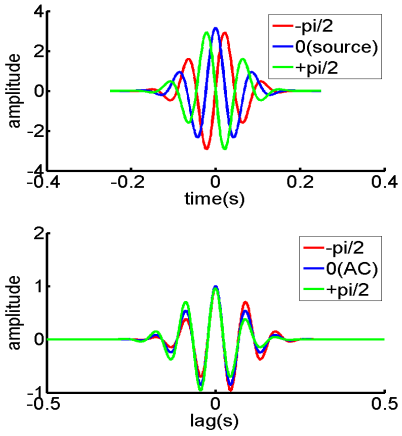

Figure 4: Phase shifted pulses (top) and their cross correlation functions (bottom)

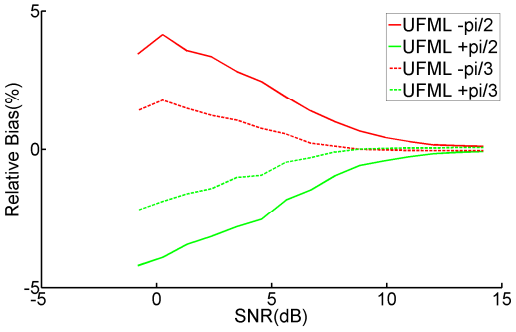

Figure5: Bias of UFML estimator pair

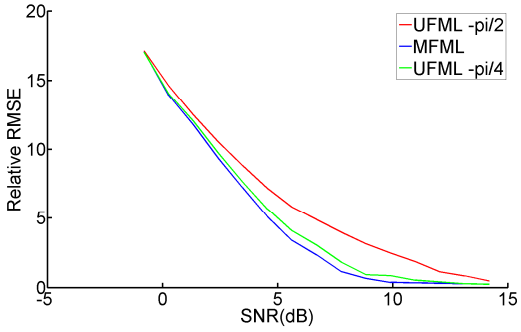

Figure 6: Relative RMSE of UMFL estimators

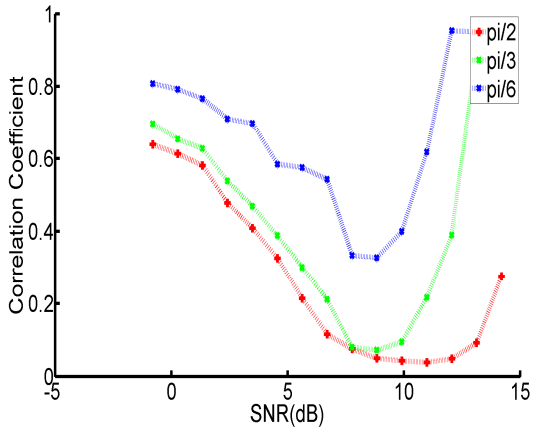

Figure 7: Cross-Correlation coefficient of UFML pair

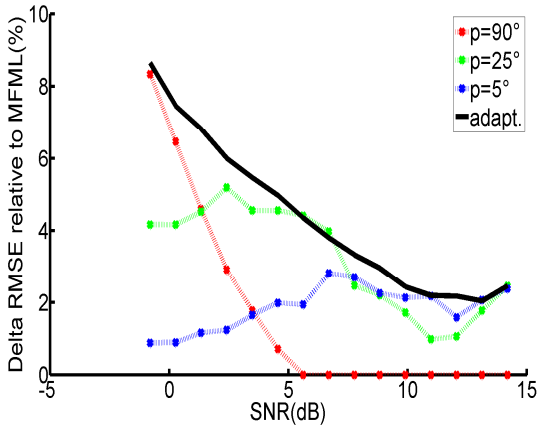

Figure 8: RMSE improvement by fixed and adaptive phase AoUFML estimators.

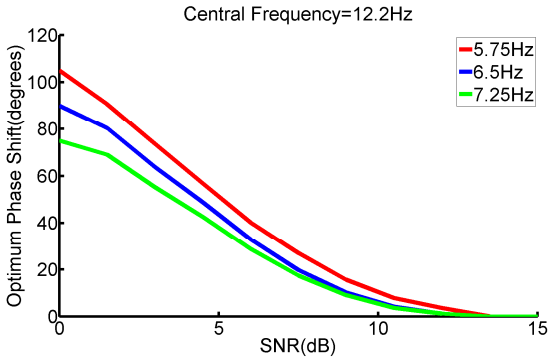

Figure 9: The optimum value of phase shift as function of SNR for different values of pulse bandwidth.

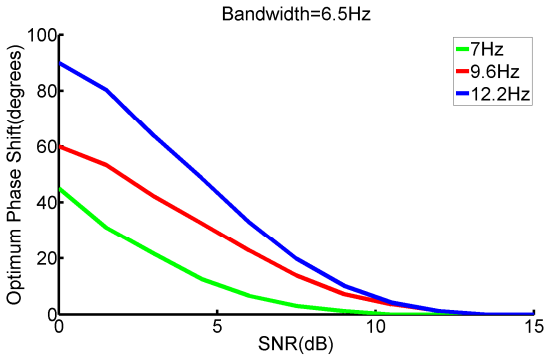

Figure 10: The optimum value of phase shift as a function of SNR for different values of pulse central frequency.